Cell Metabolism, Volume *31*

Supplemental Information

GLP-1 Receptor Signaling in Astrocytes Regulates Fatty Acid Oxidation, Mitochondrial Integrity, and Function

Katharina Timper, Almudena del Río-Martín, Anna Lena Cremer, Stephan Bremser, Jens Alber, Patrick Giavalisco, Luis Varela, Christian Heilinger, Hendrik Nolte, Aleksandra Trifunovic, Tamas L. Horvath, Peter Kloppenburg, Heiko Backes, and Jens C. Brüning

Figure S1

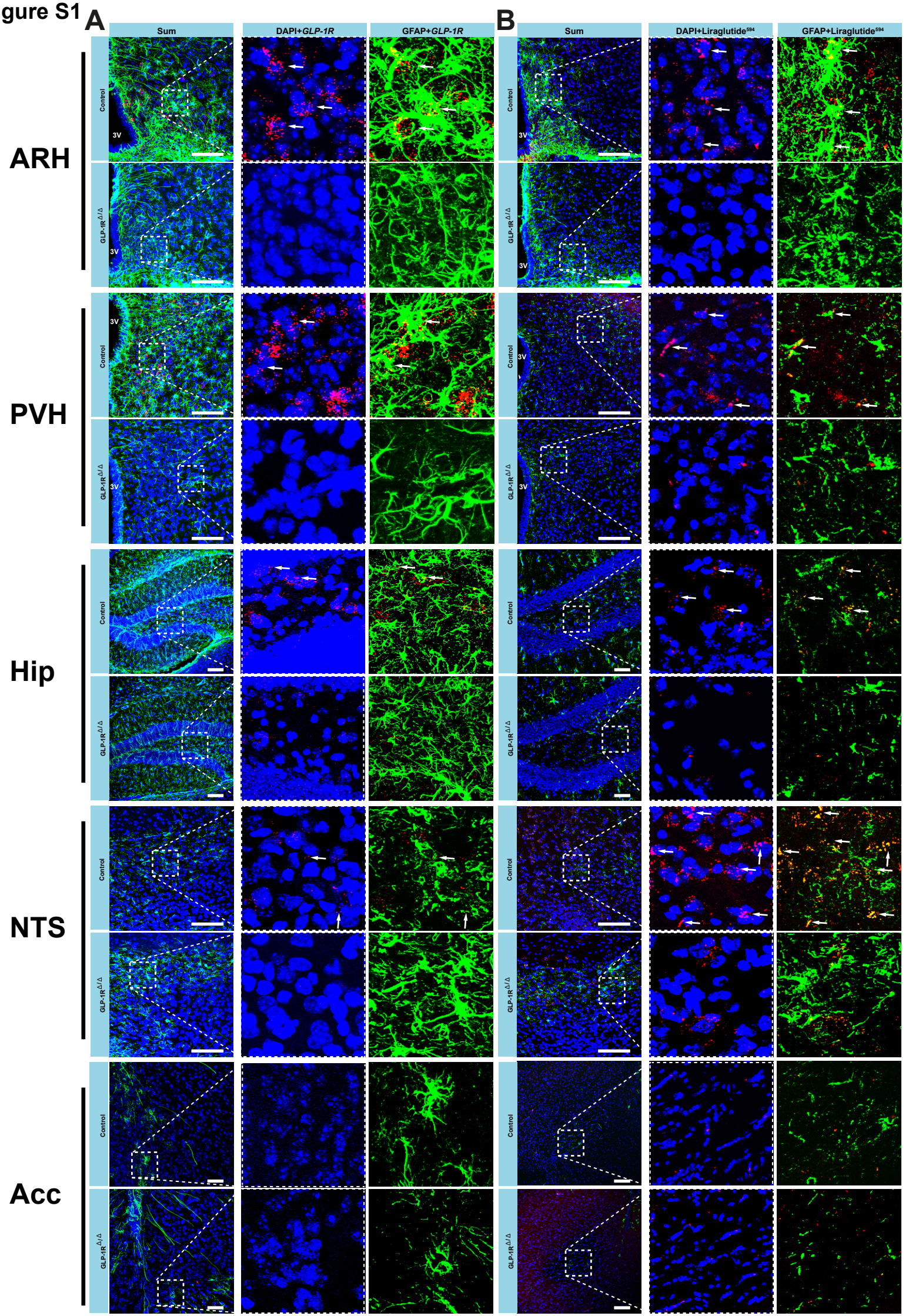
A
Sum
DAPI+GLP-1R
GFAP+GLP-1R
B
Sum
DAPI+Liraglutide594
GFAP+Liraglutide594
ARH
PVH
Hip
NTS
Acc
Control
GLP-1RΔ/Δ
3V

Figure S1

Figure S1. GLP-1R expression in astrocytes in various brain regions. Related to Figure 1.
(A) Representative confocal images of *in situ* hybridization of mRNA of *GLP-1R* (red) and immunohistochemistry detection of GFAP (green) and corresponding nuclear counterstaining (DAPI, blue) in the arcuate nucleus of the hypothalamus (ARH), the paraventricular nucleus of the hypothalamus (PVH), the hippocampus (Hip), the nucleus of the solitary tract (NTS) and the nucleus accumbens (Acc) in whole-body GLP-1R deficient mice (GLP-1R$^{\Delta/\Delta}$) and control (C57Bl6/N) mice. (B) Representative confocal images of immunohistochemistry detection of liraglutide^{594} (red) and GFAP (green) and corresponding nuclear counterstaining (DAPI, blue) in the ARH, the PVH, the Hip, NTS and the Acc in GLP-1R$^{\Delta/\Delta}$ and control mice. Arrows indicate GLP-1R;GFAP double-positive or liraglutide^{594};GFAP double-positive cells, respectively. Scale bars: 100 μm; 3V: third ventricle.

Figure S2

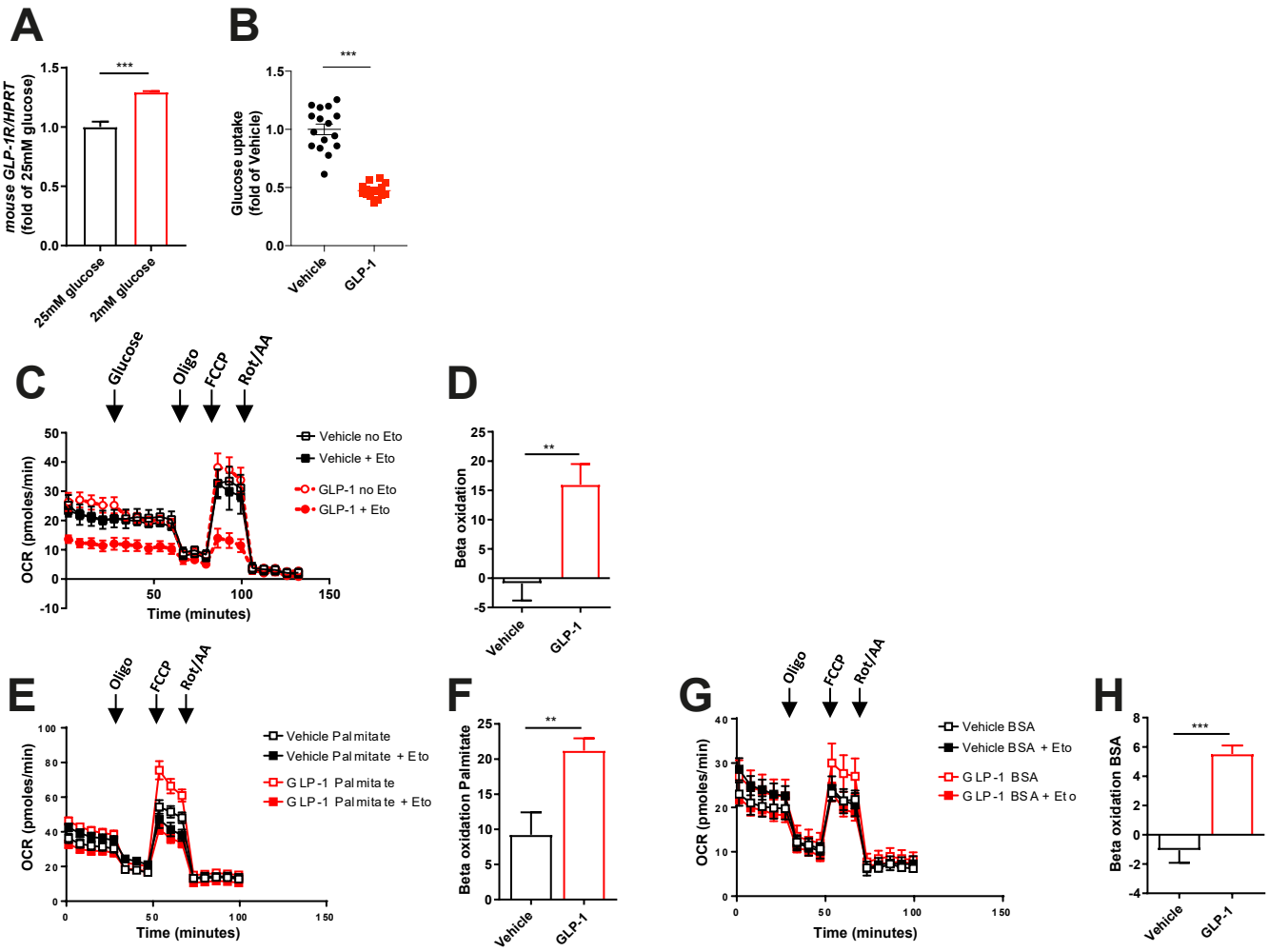

Figure S2. GLP-1 reduces glucose uptake and promotes fatty acid oxidation in primary hypothalamic astrocytes. Related to Figure 1.
(A) mRNA expression of *mouse GLP-1R* in control hypothalamic astrocytes upon 25 mM or 2mM glucose incubation (n=4 independently isolated astrocyte cultures). (B) Glucose uptake in control hypothalamic astrocytes (n=16 independently isolated astrocyte cultures). (C) Representative analysis of oxygen consumption rate (OCR) before and after glucose administration upon acute stimulation with 100 nM GLP-1 or vehicle in the presence or absence of etomoxir (Eto) in primary hypothalamic astrocytes from C57Bl6/N mice. (D) Quantification of fatty acid oxidation upon GLP-1 or vehicle treatment (beta oxidation=OCR max no Eto-OCR max + Eto; n= 8 independently isolated astrocyte cultures). (E, G) Representative analysis of OCR upon (E) palmitate or (G) BSA administration and acute stimulation with 100 nM GLP-1 or vehicle in the presence or absence of Eto. (F, H) Quantification of fatty acid oxidation upon GLP-1 or vehicle treatment in the presence of (F) palmitate or (H) BSA (beta oxidation; n= 8 independently isolated astrocyte cultures).
Data are presented as mean ± SEM. **p≤0.01, ***p≤0.001 as determined by unpaired two-tailed Student's t-test (A, B, D, F, H) .

Figure S3

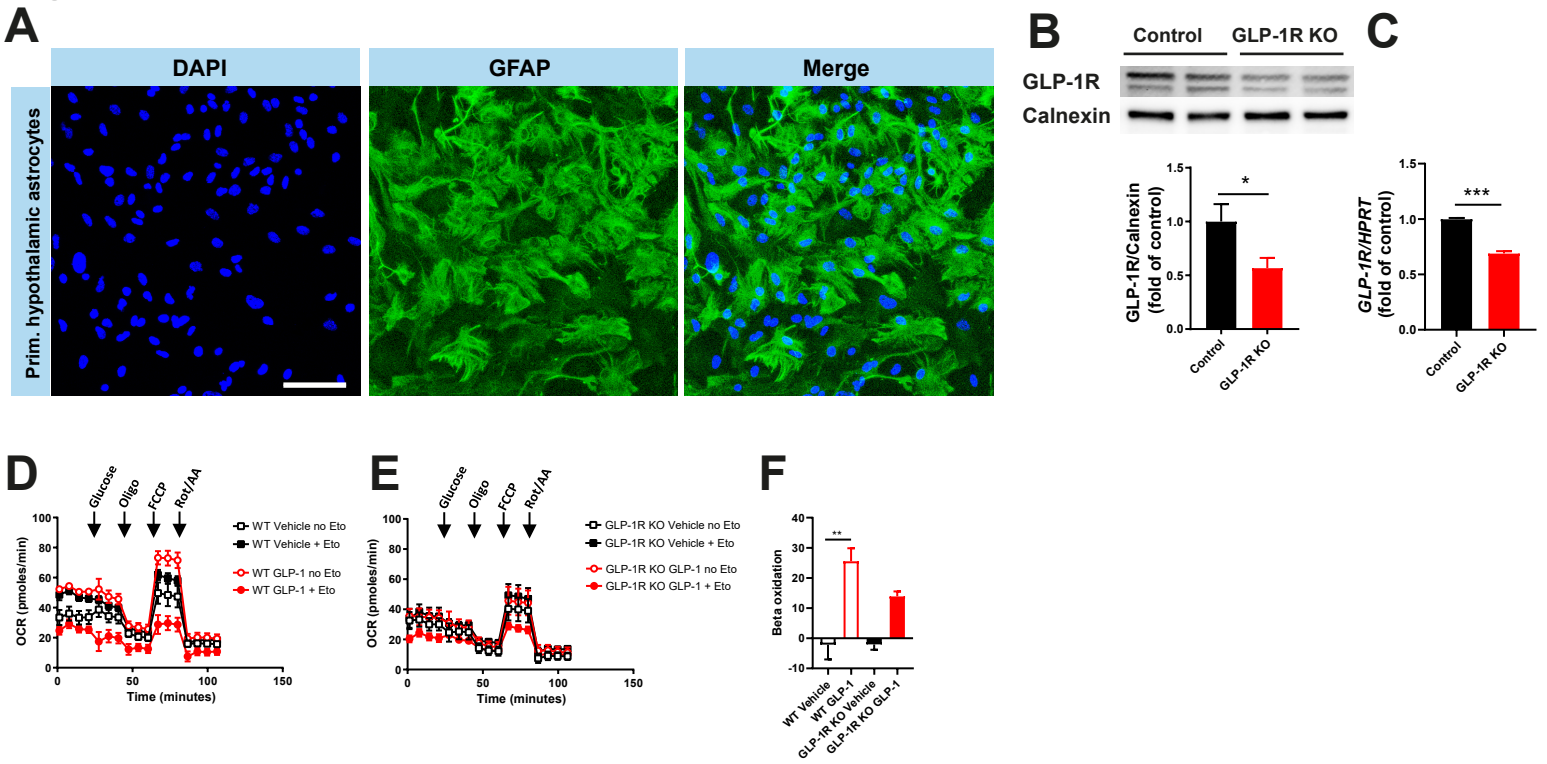

Figure S3. GLP-1R ablation in primary hypothalamic astrocytes. Related to Figure 1.
(A) Representative confocal images of immunocytochemistry detection of GFAP (green) and corresponding nuclear counterstaining (DAPI, blue) in cultured primary hypothalamic astrocytes. Scale bar: 100 µm. (B) Representative immunoblot and quantification of GLP-1R protein expression in primary hypothalamic astrocytes. Quantification of GLP-1R levels was performed after normalization to calnexin as loading control (n=4 independently isolated astrocyte cultures). (C) Quantitative analysis of *GLP-1R* mRNA expression levels in primary hypothalamic astrocytes via Real-time PCR (n=3 independently isolated astrocyte cultures). (D, E) Representative analysis of oxygen consumption rate (OCR) before and after glucose administration upon acute stimulation with 100 nM GLP-1 or vehicle in the presence or absence of etomoxir (Eto) in primary hypothalamic astrocytes from (D) control (WT), and (E) GLP-1R deficient (GLP-1R KO) mice. (F) Quantification of fatty acid oxidation upon GLP-1 or vehicle treatment (beta oxidation=OCR max no Eto-OCR max + Eto; n=3 independently isolated astrocyte cultures). Data are presented as mean ± SEM. *p≤0.05, **p≤0.01, ***p≤0.001 as determined by unpaired two-tailed Student's t-test (B, C) or two-way ANOVA followed by Bonferroni´s post-hoc test (F).

Figure S4

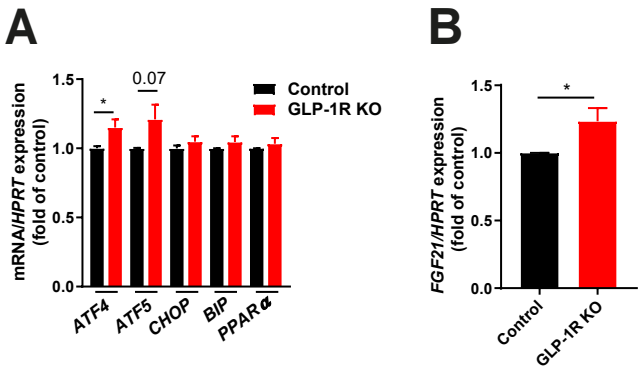

Figure S4. GLP-1R ablation induces integrated stress response genes in primary hypothalamic astrocytes. Related to Figure 1.
(A) mRNA expression of *ATF4, ATF5, CHOP, Bip*, and *PPARα* in 4 h glucose deprived (glucose 2 mM) GLP-1R-deficient (GLP-1R KO) and control primary hypothalamic astrocytes (n=7 independently isolated astrocyte cultures). (B) mRNA expression of *FGF21* in 4 h glucose deprived (glucose 2 mM) GLP-1R KO and control primary hypothalamic astrocytes (n=4 independently isolated astrocyte cultures).
Data are presented as mean ± SEM. *p≤0.05 as determined by unpaired two-tailed Student's t-test.

Figure S5

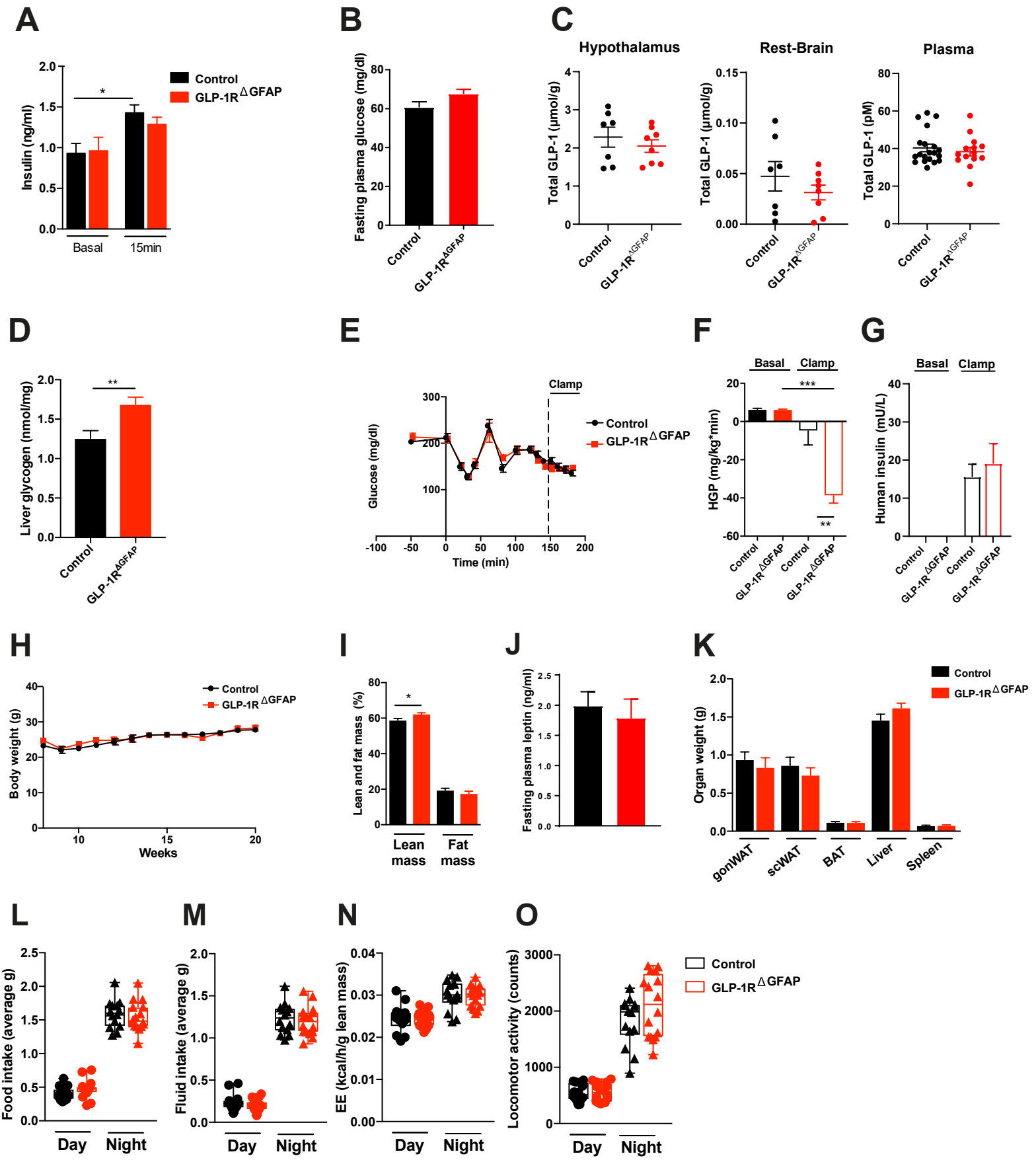

Figure S5. Reduced astrocyte GLP-1R signaling improves systemic glucose homeostasis. Related to Figure 4.

(A) Plasma insulin levels after 16 h of fasting (basal) and 15 min after intraperitoneal (ip) injection of glucose (2 g glucose per kg body weight) in GLP-1R$^{\Delta GFAP}$ and control mice (n=7 per genotype). (B) Fasting plasma glucose levels (n=15-20 per genotype) and (C) total GLP-1 levels in the hypothalamus (n=7-8 per genotype), the rest-brain (n=7-8 per genotype) and the plasma (n=14-20 per genotype) in GLP-1R$^{\Delta GFAP}$ and control mice. (D) Fasting liver glycogen levels (n=10 per genotype) in GLP-1R$^{\Delta GFAP}$ and control mice. (E) Blood glucose levels during hyperinsulinemic-euglycemic clamp studies and (F) hepatic glucose production (HGP) during the basal and clamped state in GLP-1R$^{\Delta GFAP}$ and control mice (n=9-10 per genotype). (G) Human insulin serum levels during the basal and clamped state in GLP-1R$^{\Delta GFAP}$ and control mice (n=5 per genotype). (H) Body weight development (n=10-13 per genotype), (I) body composition (n=11 per genotype), (J) fasting plasma leptin levels (n=15-20 per genotype) and (K) organ weights of perigonadal white adipose tissue (gonWAT), subcutaneous WAT (scWAT), brown adipose tissue (BAT), liver and spleen in GLP-1R$^{\Delta GFAP}$ and control mice (n=11 per genotype). (L) Food and (M) fluid intake as well as (N) energy expenditure (EE) and (O) locomotor activity as assessed via indirect calorimetry in GLP-1R$^{\Delta GFAP}$ and control mice (n=11 per genotype). EE was calculated based on lean body mass. Data are represented as mean ± SEM. *p≤0.05, **p≤0.01, ***p≤0.001 as determined by two–way ANOVA followed by Bonferroni posthoc test (A, F, G) and two-tailed, unpaired Student's t-test (D, I).

Figure S6

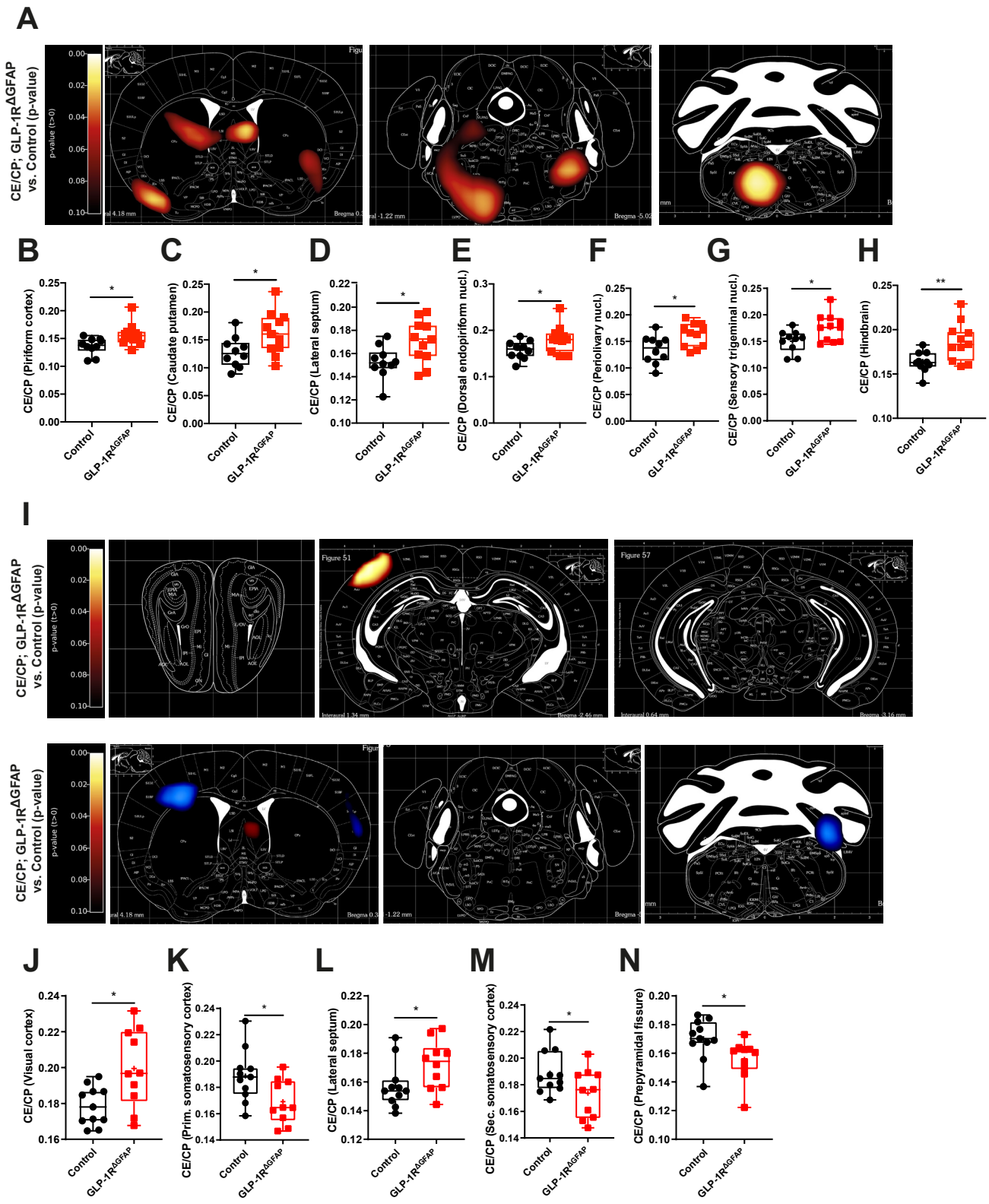

Figure S6. Astrocyte-specific GLP-1R ablation enhances brain glucose availability in response to fasting. Related to Figure 6.

(A) Images showing differential regional glucose uptake in 16 h-fasted GLP-1R$^{\Delta GFAP}$ versus control animals as determined by PET-CT. Color code represents the p value for the indicated voxels in an unpaired Student's t test in 16 h-fasted GLP-1R$^{\Delta GFAP}$ versus control animals for n=10-11 animals per genotype. Increases in glucose uptake are shown in red color. (B–H) Quantification of brain glucose uptake in 16 h-fasted GLP-1R$^{\Delta GFAP}$ versus control animals in the (B) piriform cortex, (C) caudate putamen, (D) lateral septum, (E) dorsal endopiriform nucleus, (F) periolivary nucleus, (G) sensory trigeminal nucleus, and (H) the hindbrain. (I) Images showing differential regional glucose uptake in random-fed GLP-1R$^{\Delta GFAP}$ versus control animals as determined by PET-CT. Color code represents the p value for the indicated voxels in an unpaired Student's t-test in random-fed GLP-1R$^{\Delta GFAP}$ versus control animals for n=10-11 animals per genotype. Increases in glucose uptake are shown in red color, decreases in glucose uptake are shown in blue colour. (J-N) Quantification of brain glucose uptake in random-fed GLP-1R$^{\Delta GFAP}$ versus control animals in the (J) visual cortex, (K) primary somatosensory cortex, (L) lateral septum, (M) secondary somatosensory cortex, and (N) prepyramidal fissure.

Results are presented as box plots. Upper and lower whiskers indicate the minimum and maximum values of the data, centerlines indicate the median and the mean values are represented by plus signs. *p≤0.05, **p≤0.01 as determined by unpaired two-tailed Student's t-test (B-H; J-N).

Figure S7

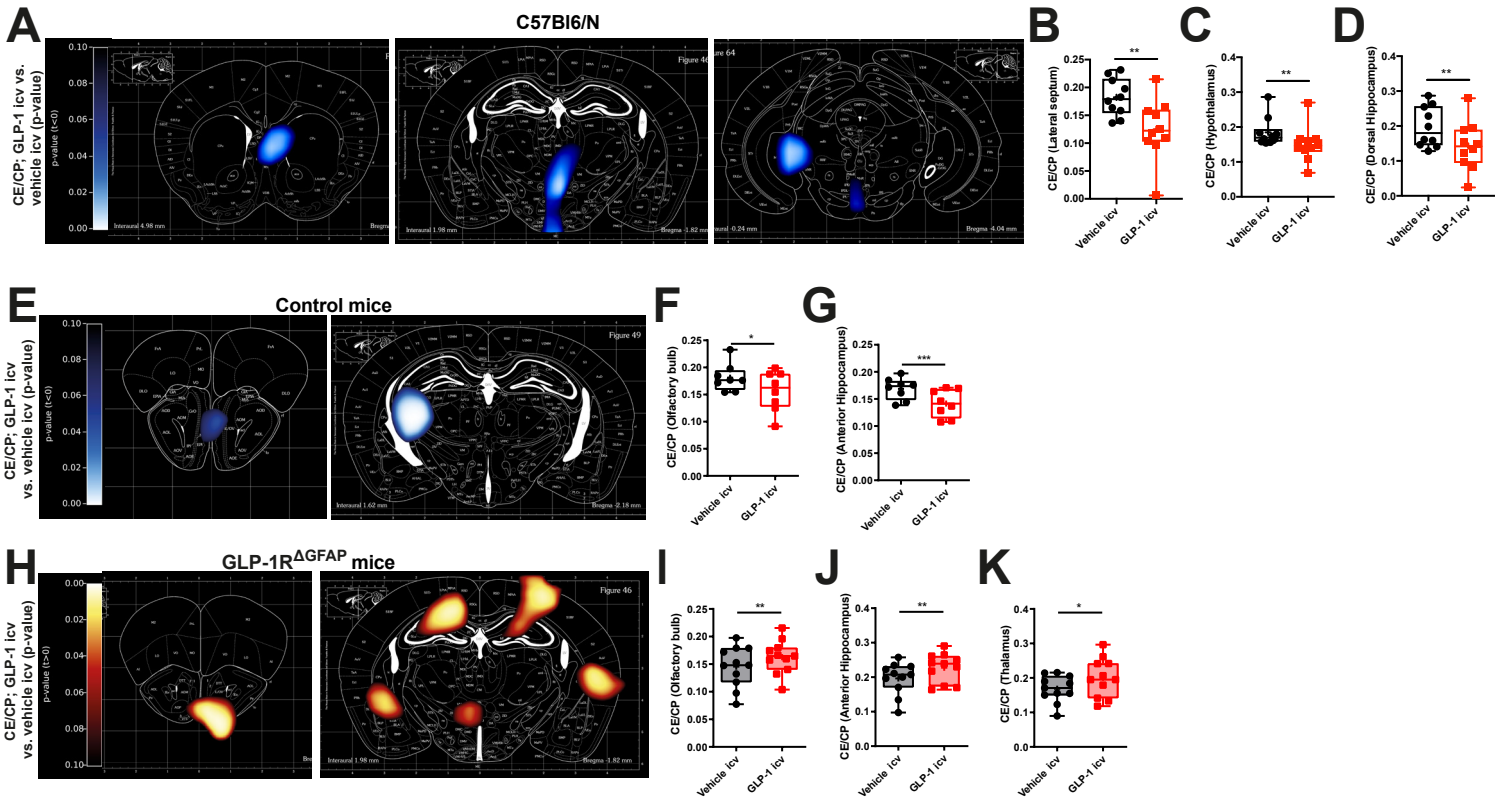

Figure S7. Central GLP-1 acutely reduces brain glucose uptake in fasted mice. Related to Figure 6.

(A, E, H) Images showing differential regional glucose uptake in 16 h-fasted (A) C57Bl6/N, (E) control and (H) GLP-1R$^{\Delta GFAP}$ mice upon intracerebroventricular (icv) injection of 1 µg GLP-1 versus vehicle as determined by PET-CT. Color code represents the p value for the indicated voxels in an unpaired Student's t test in GLP-1 versus vehicle injected animals for (A) n= 10, (E) n= 8 and (H) n= 11 animals per treatment group. Increases in glucose uptake are shown in red color, decreases are shown in blue colour. (B–D, F, G, I-K) Quantification of brain glucose uptake in 16 h-fasted (B-D) C57Bl6/N, (F, G) control and (I-K) GLP-1R$^{\Delta GFAP}$ mice acute icv injection of 1 µg GLP-1 versus vehicle in the (B) lateral septum, (C) hypothalamus, (D) dorsal hippocampus, (F) olfactory bulb, (G) anterior hippocampus, (I) olfactory bulb, (J) anterior hippocampus, and (K) thalamus.

Results are presented as box plots. Upper and lower whiskers indicate the minimum and maximum values of the data, centerlines indicate the median and the mean values are represented by plus signs. *p≤0.05, **p≤0.01, ***p≤0.001 as determined by paired two-tailed Student's t-test.

Figure S8

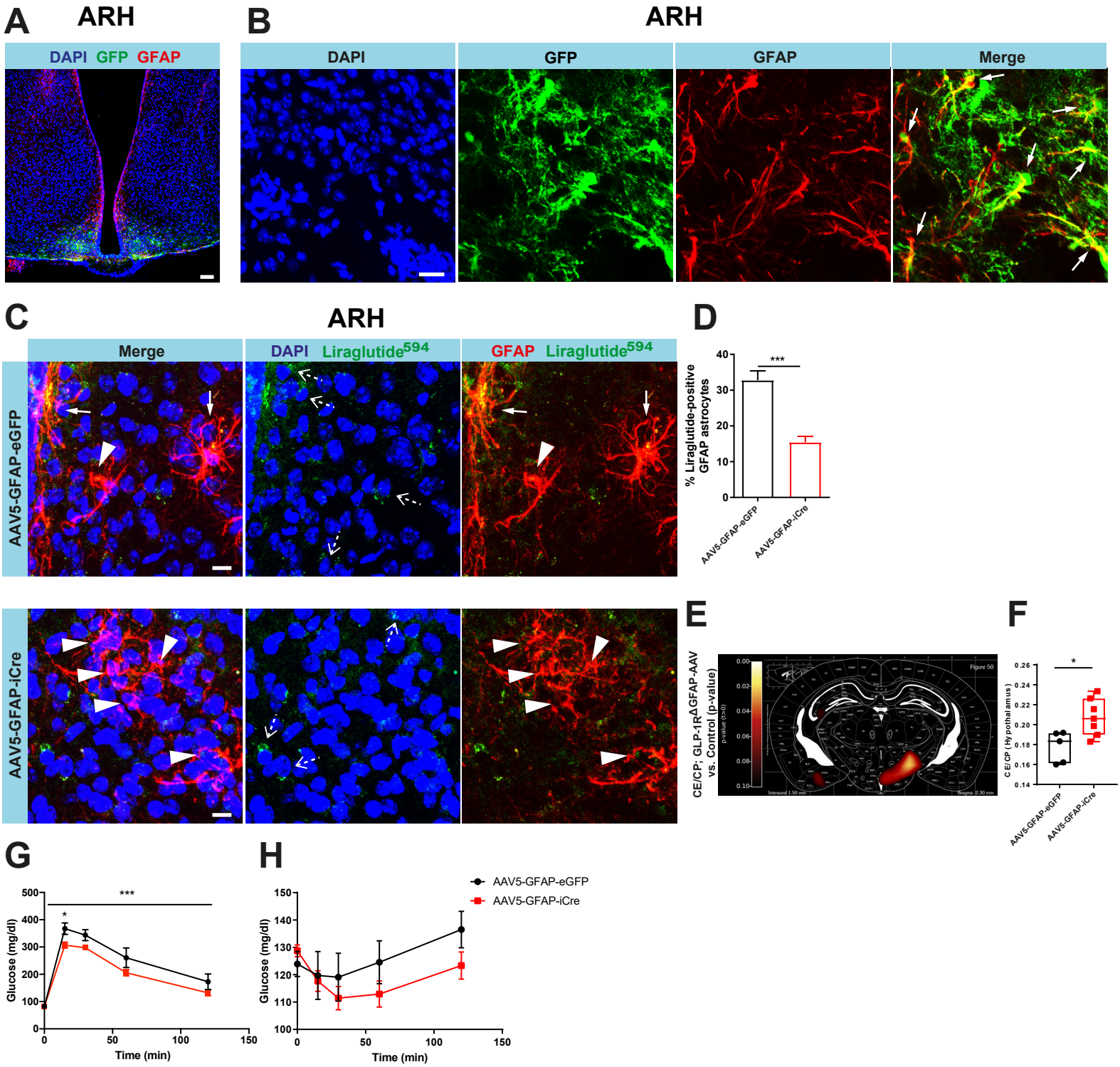

Figure S8. Reduction of GLP-1R in hypothalamic GFAP-astrocytes improves central glucose availability and systemic glucose metabolism. Related to Figure 6.

(A, B) Representative confocal images of (A) overview (Scale bar: 100 µm) and (B) detailed immunohistochemistry detection (Scale bar: 50 µm) of GFP (green), GFAP (red) and corresponding nuclear counterstaining (DAPI, blue) depicting GFP expression in the arcuate nucleus of the hypothalamus (ARH) of GLP-1R$^{flox/flox}$ mice upon ARH injection with an astrocyte-directed eGFP expressing AAV5-GFAP-eGFP. Arrows with continuous line indicating GFP expression in GFAP astrocytes. (C) Representative confocal images of immunohistochemistry detection of liraglutide^{594} (green) and GFAP (red) and corresponding nuclear counterstaining (DAPI, blue) in the ARH of GLP-1R$^{flox/flox}$ mice upon AAV5-GFAP-eGFP (control) or AAV5-GFAP-iCre injection. Filled arrows indicating liraglutide^{594}-positive GFAP-positive astrocytes, dotted arrows indicating liraglutide^{594}-positive GFAP-negative cells and arrowheads indicating liraglutide^{594}-negative GFAP-positive astrocytes. Scale bars: 10 µm. (D) Quantification of the percentage of liraglutide^{594}-positive GFAP-positive astrocytes per hemi-ARH (n=13-17 animals per group). (E) Image showing differential regional glucose uptake in 16 h-fasted AAV5-GFAP-eGFP- or AAV5-GFAP-iCre-injected GLP-1R$^{flox/flox}$ animals as determined by PET-CT. Color code represents the p value for the indicated voxels in an unpaired Student's t test in 16 h-fasted AAV5-GFAP-eGFP- or AAV5-GFAP-iCre-injected GLP-1R$^{flox/flox}$ animals for n=5-7 animals per group. Increases in glucose uptake are shown in red color. (F) Quantification of brain glucose uptake in the hypothalamus of 16 h-fasted AAV5-GFAP-eGFP- or AAV5-GFAP-iCre-injected GLP-1R$^{flox/flox}$ animals. (G) Glucose tolerance test and (H) insulin tolerance test in AAV5-GFAP-eGFP- or AAV5-GFAP-iCre-injected GLP-1R$^{flox/flox}$ mice (n=14-19 animals per group).

Results are presented as mean ± SEM or as box plots. Upper and lower whiskers indicate the minimum and maximum values of the data, centerlines indicate the median and the mean values are represented by plus signs. *p≤0.05, ***p≤0.001 as determined by unpaired two-tailed Student's t-test (D, F) and by two–way ANOVA followed by Bonferroni posthoc test (G, H).

Figure S9

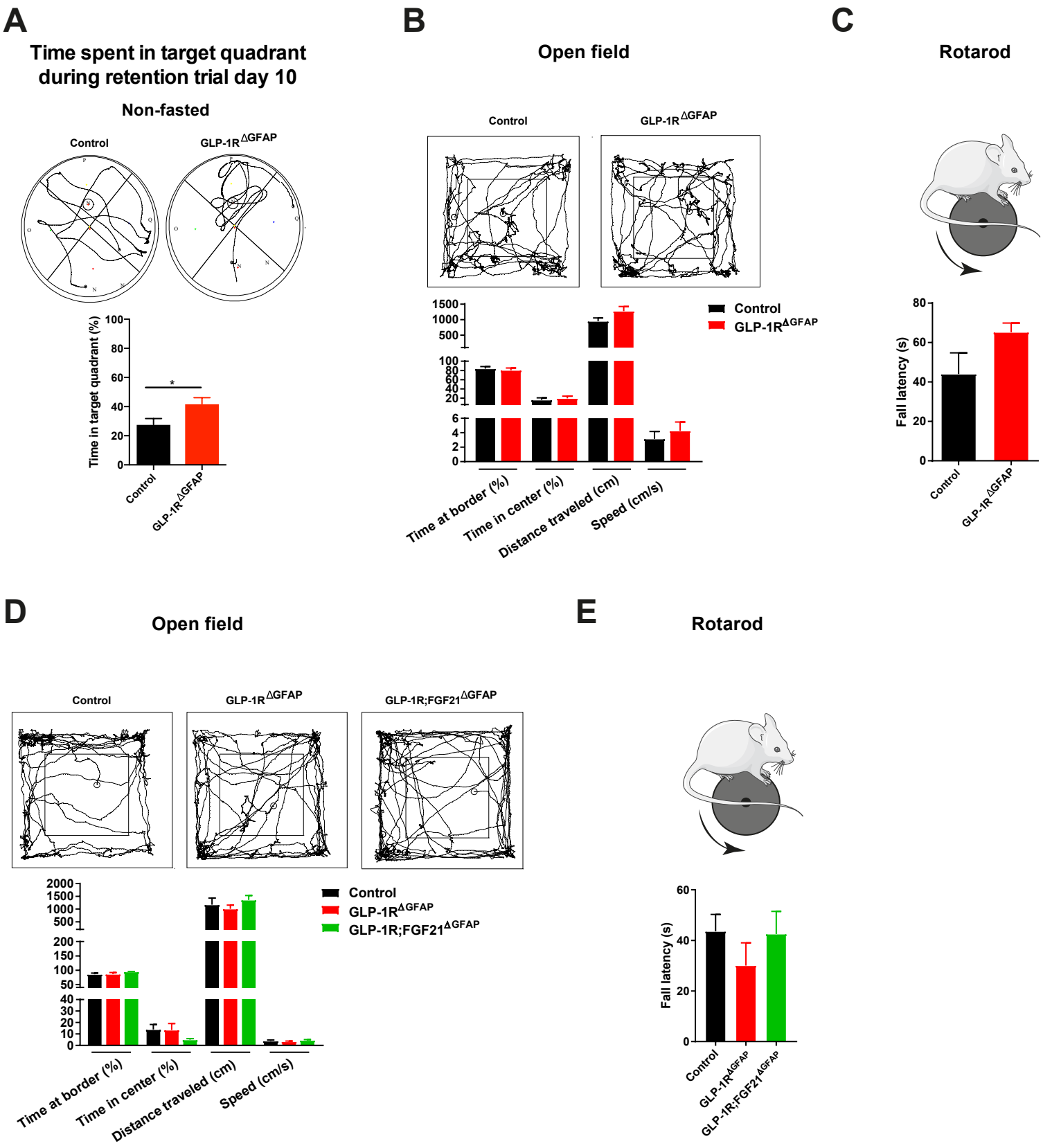

Figure S9. Astrocyte-specific GLP-1R deficiency does not alter fear, exploratory behavior or motor coordination. Related to Figure 7.
(A) Representative swimming tasks and quantification of time spent in the target quadrant during retention trial of random fed GLP-1R$^{\Delta GFAP}$ and control mice (n=9-11 per genotype) at day 10 of a Morris water maze task. (B) Representative open field tracks and quantification of % time spent at border, % time spent in center, distance traveled (in cm) and speed (in cm/s) during open field tests of GLP-1R$^{\Delta GFAP}$ and control mice (n=6-8 per genotype). (C) Fall latency during rotarod task of GLP-1R$^{\Delta GFAP}$ and control mice (n=6-8 per genotype). (D) Representative open field tracks and quantification of % time spent at border, % time spent in center, distance traveled (in cm) and speed (in cm/s) during open field tests of GLP-1R$^{\Delta GFAP}$, GLP-1R;FGF21$^{\Delta GFAP}$ and control mice (n=4-6 per genotype). (E) Fall latency during rotarod task of GLP-1R$^{\Delta GFAP}$, GLP-1R;FGF21$^{\Delta GFAP}$ and control mice (n=4-6 per genotype).
Data are represented as mean ± SEM. *p≤0.05 as determined by unpaired two-tailed Student's t-test.

Figure S10

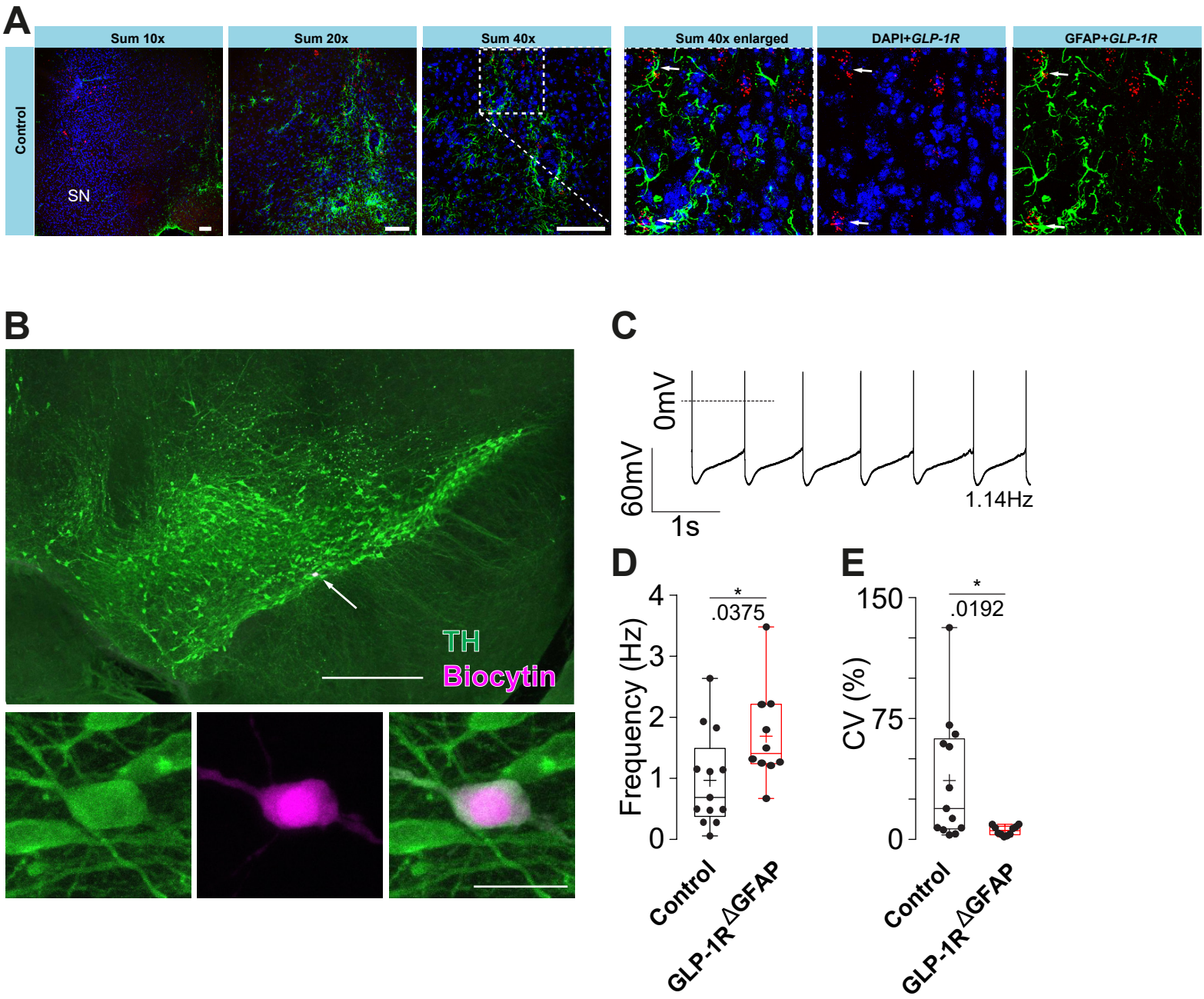

Figure S10. *GLP-1R* expression in astrocytes in close proximity to the substantia nigra (SN) and enhanced spontaneous activity of dopaminergic neurons in the substantia nigra pars compacta (SNc) of GLP-1R$^{\Delta GFAP}$ mice. Related to Figure 7.

(A) Representative confocal images of *in situ* hybridization of mRNA of *GLP-1R* (red) and immunohistochemistry detection of GFAP (green) and corresponding nuclear counterstaining (DAPI, blue) in close proximity to the substantia nigra (SN) in control mice. Arrows indicate GLP-1R;GFAP double-positive cells. Scale bars: 100 µm. (B) Upper panel: Confocal image of a recorded dopaminergic neuron (arrow) in the substantia nigra pars compacta (SNc), visualized via post hoc staining for tyrosine hydroxylase (TH) and biocytin. Scale bar: 300 µm. Lower panel: Higher magnification of the labeled neuron shown in the upper panel (left to right: TH, Biocytin, Overlay). Scale bar: 20 µm. (C) Recording from a spontaneously active SNc neuron. (D) Spontaneous firing frequency of SNc neurons recorded in brain slices from GLP-1R$^{\Delta GFAP}$ and control mice. (E) Coefficient of variation of the spontaneous activity of SNc neurons recorded brain slices from GLP-1R$^{\Delta GFAP}$ and control mice.

*$p \leq 0.05$ as determined by two-tailed, unpaired Student's t-test.